micromachines

MDPI

Article

Effect of Combustion Chamber Geometrical Parameters on the Decomposition and Combustion Characteristics of an ADN-Based Thruster

Yangyang Hou [1], Yusong Yu [1,*], Xuhui Liu [2] and Jie Cao [3]

[1] Hydrogen Energy and Space Propulsion Laboratory, School of Mechanical, Electronic and Control Engineering, Beijing Jiaotong University, Beijing 100044, China; 20116040@bjtu.edu.cn
[2] Beijing Institute of Control Engineering, Beijing 100190, China; xhliu99@163.com
[3] China North Engine Research Institute, Tianjin 300400, China; jackcao99@163.com
* Correspondence: ysyu@bjtu.edu.cn; Tel.: +86-138-1001-2475

Abstract: In this paper, numerical simulations were used to study the decomposition and combustion processes inside the 0.2 N-class ADN-based thruster, and the effects of two geometrical parameters (length and diameter) of the combustion chamber on the combustion performance were evaluated. The decomposition and combustion processes of the thruster were simulated using a reduced chemical reaction mechanism with 22 components and 20 reactions steps. According to the distribution of the basic physical fields, the variation patterns of the pressure field, velocity field, temperature field, and key component parameters caused by different combustion chamber geometrical parameters were observed and analyzed. The results show that the specific impulse and thrust of the thruster increased and then decreased with the increase of the combustion chamber diameter. When the combustion chamber diameter is 7.9 mm, the specific impulse reaches the maximum value of 206.6 s. Additionally, the specific impulse increased from 186 s to 206 s when the combustion chamber length was changed from 7 mm to 11 mm; the specific impulse increased gradually but not significantly, and the growth trend started to flatten out. The results from the paper can serve as a reference for the design and vacuum testing of an ADN-based thruster.

Keywords: ammonium dinitramide; chamber geometrical parameters; catalytic combustion; green propellant

Citation: Hou, Y.; Yu, Y.; Liu, X.; Cao, J. Effect of Combustion Chamber Geometrical Parameters on the Decomposition and Combustion Characteristics of an ADN-Based Thruster. *Micromachines* **2022**, *13*, 605. https://doi.org/10.3390/mi13040605

Academic Editors: Shizhi Qian and Teng Zhou

Received: 28 February 2022
Accepted: 11 April 2022
Published: 12 April 2022

1. Introduction

Hydrazine is widely used in the field of space propulsion, and the high-temperature mixture of ammonia, nitrogen, and hydrogen produced by their catalytic decomposition is ejected through the nozzle to produce a high specific impulse thrust [1]. However, the high vapor pressure and high toxicity of hydrazine lead to high storage, transportation, and operation costs of hydrazine propellants [2]. Therefore, the search for new nontoxic, easily stored, and structurally stable green propellants is a hot research topic in the field of propulsion and power.

The new green single-component liquid propellants mainly include hydroxylamine nitrate (HAN) single-component propellants and ammonium dinitramide (ADN) single-component propellants. ADN-based single-component propellants are high-energy ionic liquids whose high specific impulse and low toxicity are considered to be effective alternatives to hydrazine and among the most promising green propellants in the space propulsion and military fields [3,4]. The solid-state of ADN is unstable and prone to explosions due to its energy-containing substances containing reducing and oxidizing components [5–7]. Therefore, dissolving it in water to prepare an ionic solution of a certain concentration for application in green single-component engines can greatly reduce the risk of explosion. To improve the performance of the thruster, researchers added different types of fuels,

including methanol and ethanol, by considering the number of oxidant products involved in the catalytic decomposition of liquid ADN-based propellants. Swedish researchers developed an ADN-based propellant with methanol, water, and stabilizer ammonia named LMP-103S [8]. This formulation was successfully used in the High-Performance Green Propellant (HPGP) propulsion system, which was successfully applied to the Prismatic Technology Experiment (PTE) satellite on 15 June 2010, and was demonstrated in a technology demonstration [9].

The combustion of ADN-based liquid propellants is usually characterized by a series of complex physical and chemical processes, and a large number of researchers have investigated the decomposition and combustion processes of the ADN liquid phase. Yuichiro Izato et al. [10] proposed a detailed chemical kinetic model of the ADN liquid-phase reaction based on quantum chemical calculations to describe in detail the catalytic decomposition process of ADN-based liquid propellants. Their proposed new model simulates the thermal decomposition of ADN under specific heating conditions and successfully predicts the heat of reaction and the gas produced by decomposition under these conditions. Wingborg et al. [11–14] tested and evaluated the ignition characteristics, safety, stability, and purity of LMP-103S propellant by studying the ignition mode of ADN-based liquid propellant. Jing et al. [15] conducted an experimental and numerical study of the combustion process in ADN-based thrusters and found that the decomposition of ADN and the oxidation of methanol do not occur simultaneously in the reaction chamber. They pointed out that the decomposition of ADN occurs near the inlet, while methanol is oxidized downstream of the porous medium. Grönland et al. [16] found that the combustion process of aqueous ADN/methanol solution is divided into different reaction stages with different temperatures at the end of each stage. Moreover, they designed and produced catalytic particles with an appropriate activity. Later, Kamal Farhat et al. [17] investigated the catalytic decomposition process of liquid ADN using differential thermal analysis and thermogravimetric analysis methods. They demonstrated that the decomposition process occurs at a lower temperature than the decomposition temperature when no catalyst is used. Rachid et al. [18] also studied the thermal and catalytic decomposition of liquid ADN propellants and found that the addition of catalysts could effectively reduce the initial decomposition temperature of liquid ADN propellants. Meanwhile, Ju Won Kim et al. [19] measured and compared the characteristic properties and performance of different formulations of ADN-based propellants and found that the effect of catalyst active material on the propellant preheating temperature was significantly greater than that of fuel flash point and autoignition temperature.

The catalytic decomposition and combustion processes of ADN-based liquid propellants have been studied by many researchers using numerical simulations. For example, the structure of a catalytic bed filled with catalytic particles has been systematically explored and thoroughly studied [20], as well as the effect of propellant components and ratios on the decomposition and combustion process of thrusters [21]. It can be found that although the abovementioned literature describes the ADN-based propellant decomposition combustion, there are fewer studies on the changes in combustion characteristics of thrusters caused by some specific factors. In the present work, we investigate the effect of combustion chamber geometrical parameters on the spray, evaporation, heat, and mass transfer within the catalytic bed, catalytic decomposition, and combustion processes in a single-component thruster model. The Rosin–Rammler model was used to determine the distribution of ADN droplet particle size. The effective thermal conductivity is added to the energy equation to simulate the complex heat transfer process in porous media. Finally, the decomposition and combustion processes of ADN-based liquid propellants and the effects of different combustion chamber geometrical parameters on the propellant performance are investigated.

The combustion chamber, where the high-temperature combustion reaction of methanol happens, is an important component structure of the ADN-based thruster, and its main geometric parameters play an important role in the internal decomposition and combustion

process of the ADN-based thruster. In this paper, numerical simulation is used to carry out the optimized design of ADN-based thruster combustion chamber geometry to provide data reference for the performance optimization of high-performance ADN-based thrusters.

2. Description of Numerical Simulations and CFD Methods

2.1. Thruster Geometry and Calculation Settings

In this paper, the influence of the combustion chamber geometrical parameters on the internal decomposition and combustion characteristics of the thruster is investigated by three-dimensional numerical simulation. Figure 1a shows the geometric model of the thruster. The DPM method is used to simulate the movement of droplets within the catalytic bed. The resistance of the catalytic bed to the droplet is loaded onto the droplet by the UDF function of the fluent software. The Rosin–Rammler model was used to describe the distribution of droplets within the catalytic bed. The droplet composition is an ADN-based liquid propellant, where the mass fraction ratio of ADN, AN, H_2O, and CH_3OH is 50%:14%:18%:18%.

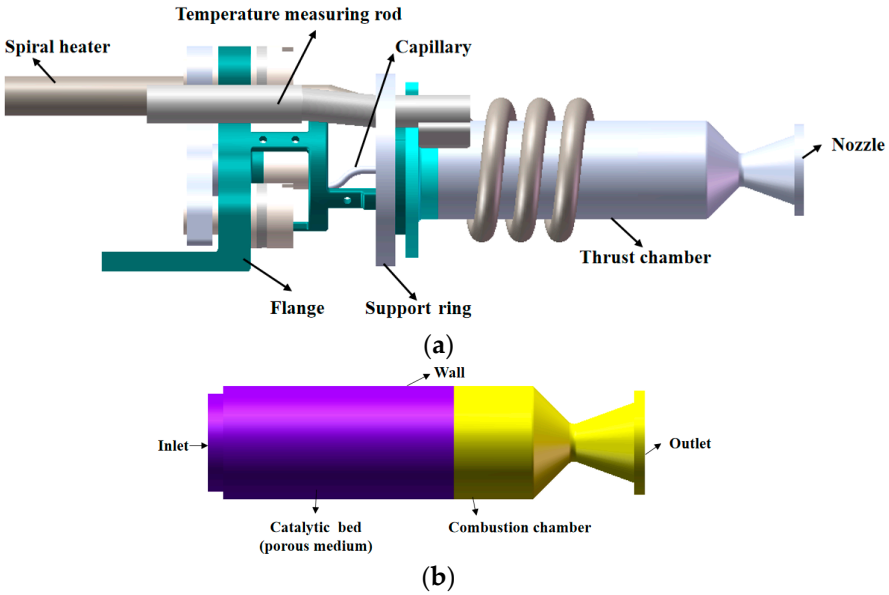

Figure 1. Geometric model of ADN thruster: (**a**) geometric structure; (**b**) computational domain.

The pressure solver was chosen and was a second-order implicit solver. The apparent velocity solver was used for porous media. The SIMPLE algorithm was used. The outer wall surface of the thruster was a radiation boundary condition. The inlet mass flow rate of the ADN thruster was 0.1 g/s. The porosity and initial temperature of the catalytic bed were 0.275 and 200 °C. The wall temperature was measured by the test, the wall temperature of the catalytic bed was 700 °C, and the wall temperature of the combustion chamber was 900 °C. The geometric parameters of the ADN-based thruster are listed in Table 1.

Table 1. The geometry parameters of ADN-based thruster.

	Parameter	Value
Thruster geometry parameters	Catalyst bed length (m)	1.5×10^{-2}
	Catalyst bed diameter (m)	6.9×10^{-3}
	Combustion chamber length (m)	5.3×10^{-3}
	Combustion chamber diameter (m)	6.9×10^{-3}
	Nozzle expansion ratio	50

As shown in Figure 2, the grid independence analysis is carried out using five mesh resolutions: very coarse, coarse, medium, fine, and very fine grid. The average combustion

chamber temperature is compared as the basis for the grid independence study. The minimum gird size can be refined down to 2.5 um and 1 um in the nozzle zone for the fine and very fine mesh cases, respectively. The relative derivation is calculated from the results of a very fine grid. The results show that the relative deviations for grid numbers of 20,000, 40,000, 80,000, and 120,000 are 12.3%, 9.25%, 4.61%, and 0.94%, respectively. We think that the relative deviation within 1% has a relatively small effect on the calculation results. When the grid number exceeds 120,000, it can be approximated that the temperature tends to be stable. In this study, we consider a fine grid to be the most appropriate in order to reduce the computational time.

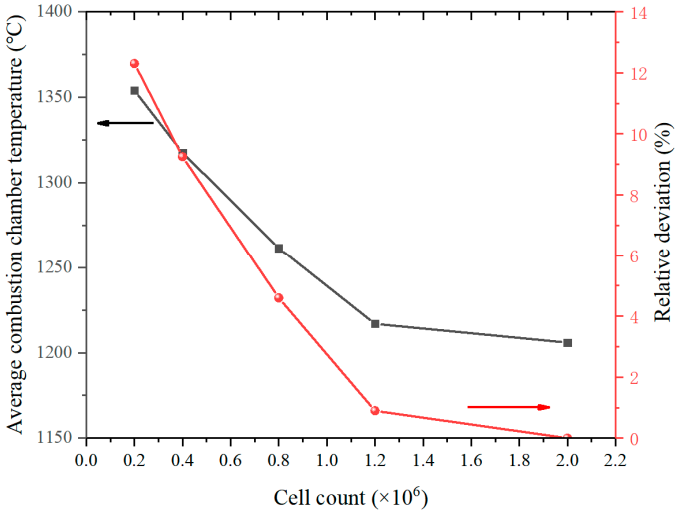

Figure 2. Comparison of average combustion chamber temperature and relative deviation for different cell counts.

2.2. Numerical Description

The structure of the catalytic bed is complex, and the distribution pattern is random. Therefore, the catalytic particles are assumed to be spherical particles in a virtual porous medium in the established model. The droplet distribution model for atomization was selected for numerical simulation from the Rosin–Rammler model. The literature [20] has validated the Rosin–Rammler model as the appropriate spray model for this study. The droplet distribution function of the Rosin–Rammler model is based on the assumption of an exponential relationship between the droplet diameter d and the mass fraction Yd of the droplets with diameters exceeding d. This exponential relationship is as follows.

$$Yd = e^{-(d/\overline{d})^n} \quad (1)$$

where $\overline{d}$ is the mean diameter, and n is the propagation parameter used to define the droplet size distribution in the Rosin–Rammler model. The value of n was given in Table 2.

Table 2. The characteristics of the ADN-based propellant and key equation coefficients.

	Value	Literature
Density of liquid (kg/m^3)	1290	[3]
Cp (Specific Heat) (J/kg·k)	2350	[3]
Viscosity (kg/m·s)	0.0046	[3]
n	7.726	[20]
d (μm)	80.7	[20]
γ	0.5	[21]
k_f(W/m·K)	0.8	[22]
k_s(W/m·K)	25.1	[22]

A multicomponent liquid evaporation model was used to describe the evaporation process of ADN-based propellants. In this case, the multicomponent droplet evaporation rate is the result of summing the evaporation rates of individual components [23].

The evaporation rate of component i is calculated by the following equation:

$$\frac{dm_i}{dt} = A_p M_{w,i} k_{c,i} (C_{i,s} - C_{i,\infty}) \tag{2}$$

where m_i is the mass of component i in the droplet, $k_{c,i}$ is the mass transport coefficient of component i, A_p is the surface area of the droplet, $M_{w,i}$ is the molecular weight of component i, and $C_{i,s}$ and $C_{i,\infty}$ are the concentrations of component i on the droplet surface and inside the droplet.

When the total evaporation pressure on the droplet surface exceeds the room pressure, the multicomponent droplet is in a boiling state. The total evaporation pressure is calculated using the formula $P_t = \sum P_i$, where P_i is the partial pressure of component i [24].

The boiling rate equation:

$$\frac{dm_i}{dt} = x_i \frac{\pi d_p k_\infty}{c_{p\infty}} \left(2 + 0.6 Re_d^{1/2} Pr^{1/3}\right) \ln(1 + B_{T,i}) \tag{3}$$

where x_i is the volume fraction of component i in the droplet, d_p is the droplet diameter, k_∞ is the thermal conductivity of the continuous phase, $c_{p\infty}$ is the specific heat capacity of the continuous phase, and $B_{T,i} = \frac{c_{p\infty}\left(T_\infty - T_p\right)}{h_{vap,i}}$ is the Spalding heat transfer coefficient of component i.

In order to comprehensively describe the heat exchange process occurring in porous media, the effective thermal conductivity and the corresponding source term are added to the energy equation to model the complex heat transfer process in porous media. Due to the large temperature difference between the solid and fluid phases, the thermal conductivity between the fluid and the solid needs to be considered simultaneously, and a local nonthermal equilibrium model can be used to establish a nonisothermal model for the porous media region [25,26].

Fluid zone energy conservation equation:

$$\begin{aligned} &\tfrac{\partial}{\partial t}(\gamma \rho_f E_f) + \nabla \cdot (\vec{v}\left(\rho_f E_f + p\right)) \\ &= \nabla \cdot \left(\gamma k_f \nabla T_f - \left(\sum_i h_i J_i\right) + \left(\vec{\tau} \cdot \vec{v}\right)\right) + S_f^h + h_{fs} A_{fs}\left(T_f - T_s\right) \end{aligned} \tag{4}$$

Solid zone energy conservation equation:

$$\frac{\partial}{\partial t}((1-\gamma)\rho_s E_s) = \nabla \cdot ((1-\gamma) k_s \nabla T_s) + S_s^h + h_{fs} A_{fs} (T_f - T_s) \tag{5}$$

where the subscripts f and s represent fluid and solid, γ is the porosity of porous media, k_f is the fluid-phase thermal conductivity, k_s is the solid-phase thermal conductivity, h_{fs} is the thermal conductivity between fluid and solid, and A_{fs} is the fluid–solid interfacial density.

It is also necessary to model the heat–fluid–solid coupling in the thruster [27,28].

The solid zone heat transfer conservation equation is:

$$\frac{\partial}{\partial t}(\rho h) + \frac{\partial}{\partial x_i}(\rho u_i h) = \frac{\partial}{\partial x_i}\left(k \frac{\partial T}{\partial x_i}\right) + q^m \tag{6}$$

where ρ is the solid density, h is the sensible enthalpy, k is the solid heat transfer coefficient, T is the temperature, and q^m is the volume source term.

Fluid–solid coupling cross-interface equation; similarly, the fluid–solid coupling follows the most basic conservation principle, so at the fluid–solid coupling interface, the fluid–solid heat flow q conservation should be satisfied as follows:

$$q_f = q_s \tag{7}$$

The kinetic model for the catalytic decomposition and combustion reaction of ADN/methanol propellant includes 22 components and 20 primitive reactions (Table 3) [29–31]. The equations describing the catalytic reactions are solved using a surface reaction approach. Since the catalytic bed area is modeled using the actual particle filling method, the surface reaction rate can be found by simply solving the energy equation to find the current surface temperature of the particles, giving the activation energy of the surface reaction, the pre-exponential frequency factor, and the surface adsorption enthalpy, and determining the concentration and pressure of the reaction components in the fluid near the particle surface. In order to improve the calculation rate, this study will use the processing of particle surface partitioning to speed up the solution of the surface reaction.

Table 3. Twenty-step chemical reaction model of ADN/methanol [20,21,30].

$ADN(G) + M => NH_3 + HN_3O_4 + M$	$CH_3OH + OH = CH_2OH + H_2O$
$HN_3O_4 = HNNO_2 + NO_2$	$CH_2OH + O = CH_2O + OH$
$2CH_3OH + 2NO_2 = 2HCOOH + N_2 + 2H_2O$	$CH_2O + OH = HCO + H_2O$
$HNNO_2 + M = N_2O + OH + M$	$HCO + OH = H_2O + CO$
$NH_3 + OH = NH_2 + H_2O$	$H_2NO + O = NH_2 + O_2$
$OH + OH = H_2O + O$	$NH_2 + NO = N_2 + H_2O$
$HNNO_2 + OH = H_2O + 2NO$	$N_2O + M = N_2 + O + M$
$NH_2 + NO_2 = H_2NO + NO$	$N_2O + O = N_2 + O_2$
$NO + NO = N_2 + O_2$	$2HCOOH + O_2 = 2CO_2 + 2H_2O$
$CH_3OH + O_2 = CH_2OH + HO_2$	$CO + O + M = CO_2 + M$

2.3. 0.2 N-Class ADN-Based Thruster Vacuum Ground Test

The test data were supported by the Beijing Institute of Control Engineering. Figure 3 shows the vacuum ignition test system of the ADN-based liquid thruster. The thruster is divided into four main parts: solenoid valve, injector, thrust chamber, and thermal control assembly. The solenoid valve realizes the switch control of the propellant; the injector plays the role of blocking the heat of the thrust chamber and carrying out the flow pressure drop control, using a single capillary injection heat-conducting structure. The thrust chamber includes the catalytic bed and the combustion chamber, and the catalytic bed is filled with granular catalyst, which plays the role of catalytic decomposition of the propellant. The noble metal iridium-based catalyst was used as a catalytic bed, and the particle size was 30 mesh. The catalytic particles are loaded into the catalytic bed using a vibratory filling method. The combustion chamber is located downstream of the catalytic bed for further combustion reactions. The thermal control assembly includes an armored heater and a temperature measuring platinum resistor, micro thruster design rated vacuum steady-state thrust 0.2 N, rated flow 0.1 g/s, and rated vacuum-specific impulse greater than 200 s. Green nontoxic ADN propellant consists of ADN, methanol, and water in a certain ratio. When the propellant enters the preheated catalytic bed, ADN decomposes under the catalytic action, and a large amount of oxidizing intermediate products produced by the decomposition of ADN and methanol in the propellant are further burned to release a large amount of heat. The high-temperature gas is ejected through the tail nozzle to generate thrust. The temperature and thrust curves of the thruster are shown in Figures 4 and 5. The case temperatures of the catalytic bed and combustion chamber were measured by the temperature sensors mounted on the thruster at about 720 °C and 1010 °C.

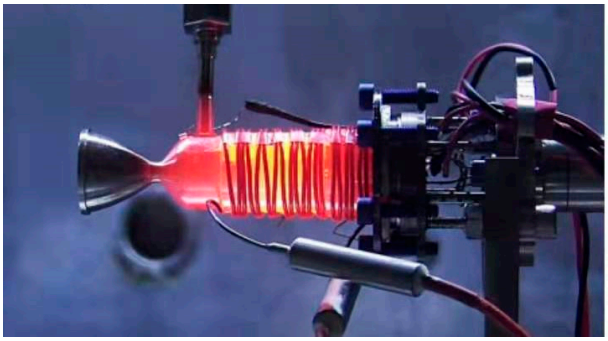

Figure 3. The appearance of the ADN-based thruster including four parts: solenoid valve, injector, catalytic bed, combustion chamber, and nozzle.

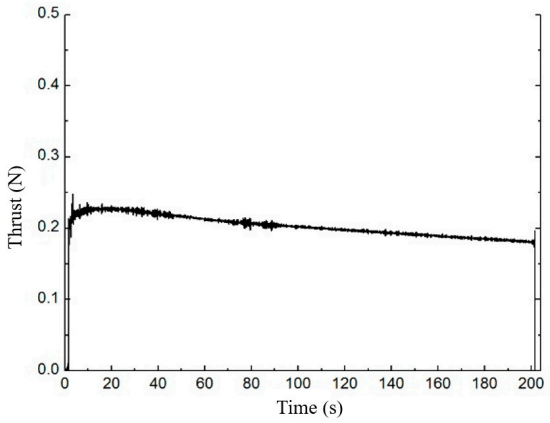

Figure 4. 200 s steady-state thrust of 0.2 N-class thruster.

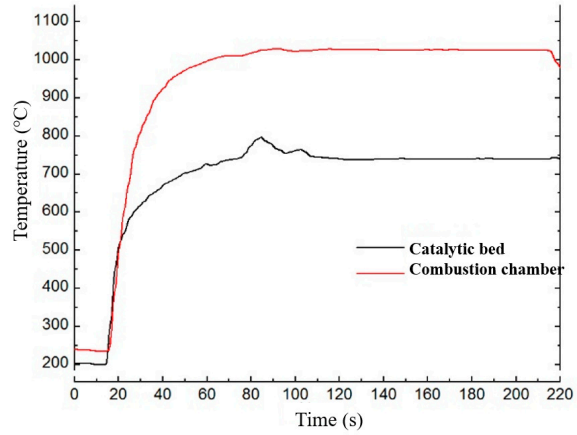

Figure 5. The temperature of catalytic bed and combustion chamber of 0.2 N-class thruster.

2.4. Model Validation

In order to verify the correctness of the thruster model, a comparative study with the temperature of the thruster in the ground vacuum thermal test was conducted. The vacuum ground test data were provided by the Beijing Institute of Control Engineering. The comparison curve of the case temperature of the thruster is shown in Figure 6, and Table 4 shows the comparison results of the numerical simulation and the test under 60 s steady-state conditions. The results show that the combustion chamber temperatures of test and simulation under steady-state conditions are 1013 °C and 1004 °C, with errors less than 5%, which meet the accuracy requirements.

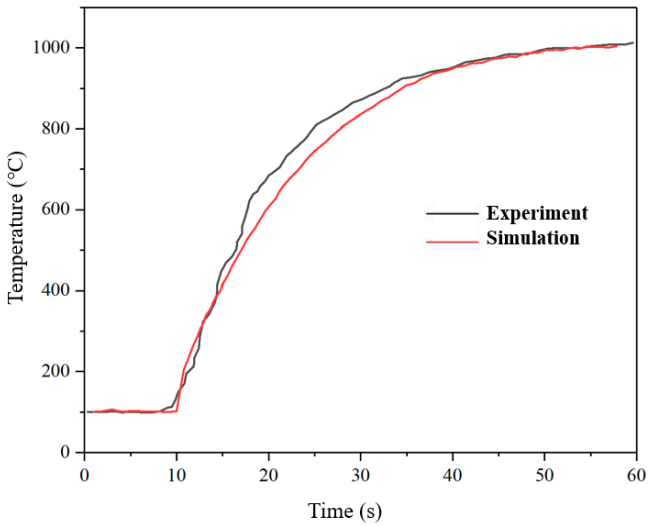

Figure 6. Comparison between simulation and experiment.

Table 4. Comparison between experimental results and simulation results under 60 s steady-state conditions.

	Experimental Result	Numerical Result	Error
Mean thrust (N)	0.21	0.203	3.33%
Temperature of combustion chamber (°C)	1013	1004	0.89%
Temperature of catalytic bed (°C)	706	721	2.12%

3. Results and Discussion

3.1. Catalytic Decomposition and Combustion Processes in ADN-Based Thrusters

In this paper, the decomposition reaction of ADN propellant and the oxidizer combustion process in the ADN thruster are simulated. As shown in Figure 7, the change laws of temperature, pressure, velocity, and concentration of various component substances in the thruster are analyzed. As shown in Table 5, the peak temperature of the combustion chamber is 1800 K. The high-temperature region of the combustion chamber is concentrated near the nozzle exit. The region after the heating up, including the back of the catalytic bed and the combustion chamber, is kept in the high-temperature region. In the tapering section of the nozzle, the temperature continues to drop until the gas stream exits the nozzle. The pressure distribution shows that the pressure in the catalytic bed and combustion chamber can reach 0.94 MPa after the complete combustion of ADN/methanol propellant, and the pressure continues to decrease after the nozzle tapering section. The thrust value of the ADN thruster obtained from the simulation is 0.202 N. Compared with the velocity at the nozzle exit, the velocity in the catalytic bed and combustion chamber is lower, and the velocity of the gas passing through the nozzle is accelerated. The maximum velocity at the exit of the nozzle is about 2100 m/s. The velocity increases rapidly at the axial position of the tapering section of the nozzle due to the wall viscosity, and the velocity is lower near the wall of the nozzle. The decomposition reaction of ADN occurs immediately after entering the catalytic bed, and the decomposition rate of ADN near the wall is slower than that in the center of the catalytic bed due to the wall effect, and the ADN is basically consumed in the 1/2~1/3 area of the catalytic bed, and the HN_3O_4, methanol, and formic acid produced by the decomposition mainly exist in the front half of the catalytic bed. The reaction products OH were mainly distributed in the combustion chamber and nozzle area, and N_2O and O_2 were distributed in the latter half of the catalytic bed and the front part of the combustion chamber.

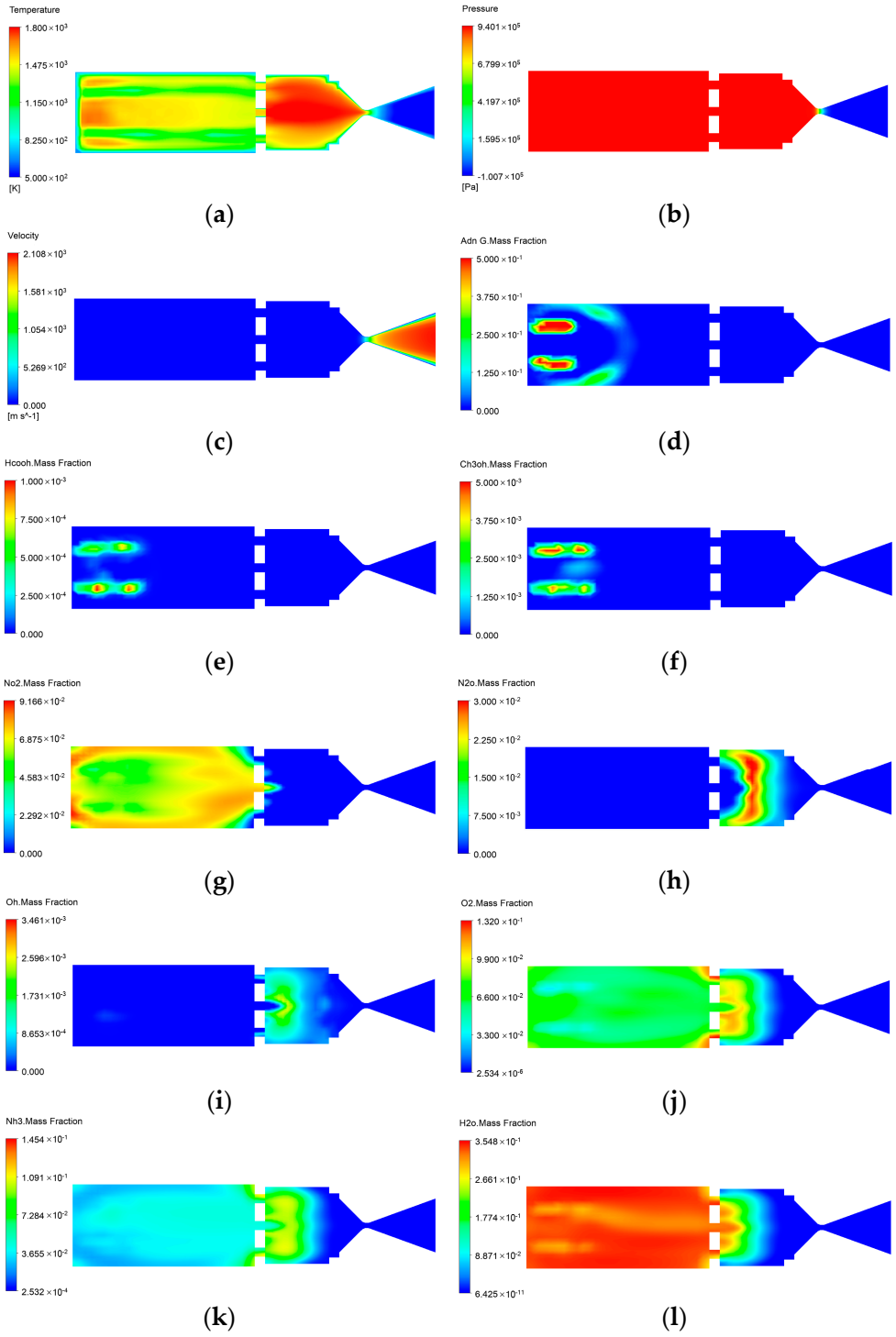

Figure 7. Distributions of important physical fields within the ADN-based thruster: (**a**) temperature; (**b**) pressure; (**c**) velocity; (**d**) ADN mass fraction; (**e**) HCOOH mass fraction; (**f**) CH_3OH mass fraction; (**g**) NO_2 mass fraction; (**h**) N_2O mass fraction; (**i**) OH mass fraction; (**j**) O_2 mass fraction; (**k**) NH_3 mass fraction; (**l**) H_2O mass fraction.

Table 5. Key parameters of ADN-based thrusters in the middle of the catalytic bed and the combustion chamber.

	Middle of the Catalytic Bed	Middle of the Combustion Chamber
temperature (°C)	1126	1525
Pressure (MPa)	0.96	0.94
Velocity (m/s)	43	86
ADN mass fraction	0.25	6×10^{-3}
HCOOH mass fraction	6.1×10^{-4}	9.4×10^{-5}
CH_3OH mass fraction	0.03	0.025
NO_2 mass fraction	2.4×10^{-5}	1.3×10^{-5}
N_2O mass fraction	3.6×10^{-3}	5×10^{-4}
OH mass fraction	5×10^{-4}	2.3×10^{-3}
O_2 mass fraction	4.3×10^{-5}	1.9×10^{-5}
NH_3 mass fraction	0.04	0.073
H_2O mass fraction	0.28	0.16

3.2. Effect of Combustion Chamber Diameter on Thruster Decomposition and Combustion Characteristics

The combustion chamber diameter affects the oxidation reaction process inside the combustion chamber and also the propellant flow and heat and mass transfer characteristics inside the combustion chamber. The results of the internal temperature, velocity, and spatial distribution of the main reaction components of the ADN-based thruster at steady-state operation are given in Figure 8. In this work, the decomposition and combustion characteristics of the thruster will be investigated for combustion chamber diameters of 4.9 mm, 5.4 mm, 5.9 mm, 6.4 mm, 6.9 mm, 7.4 mm, 7.9 mm, 8.4 mm, and 8.9 mm.

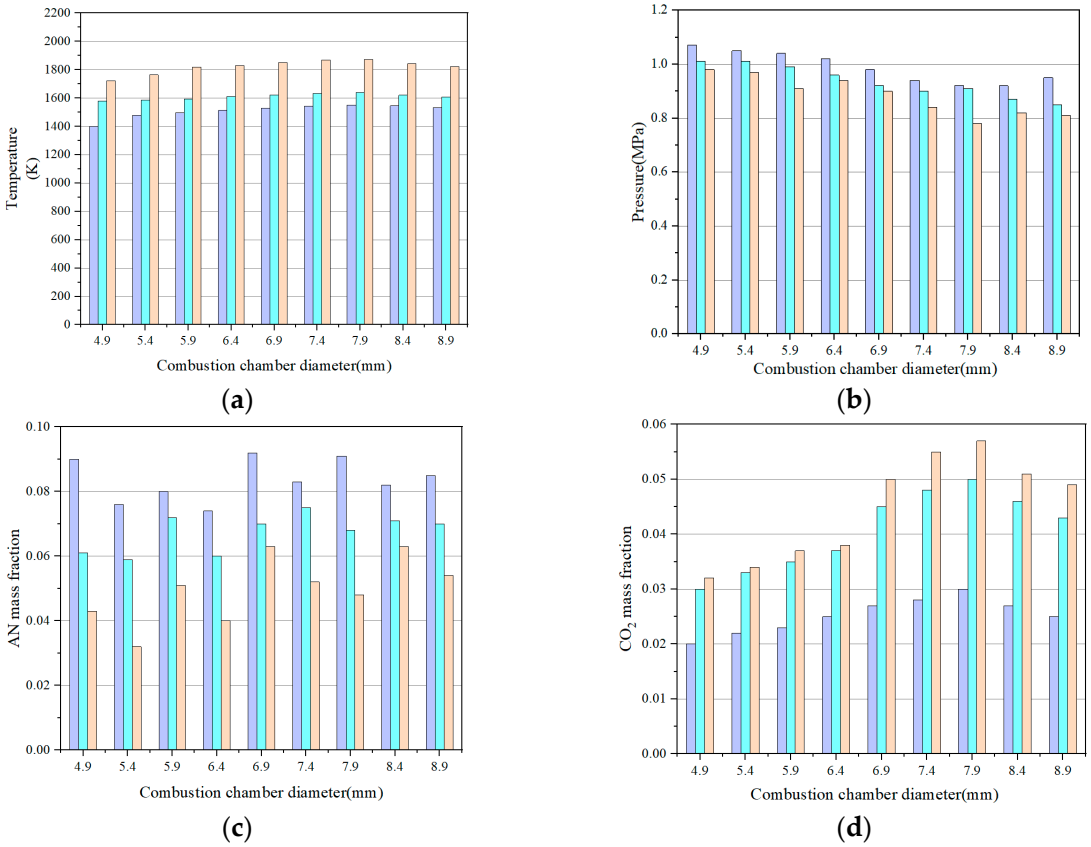

Figure 8. *Cont.*

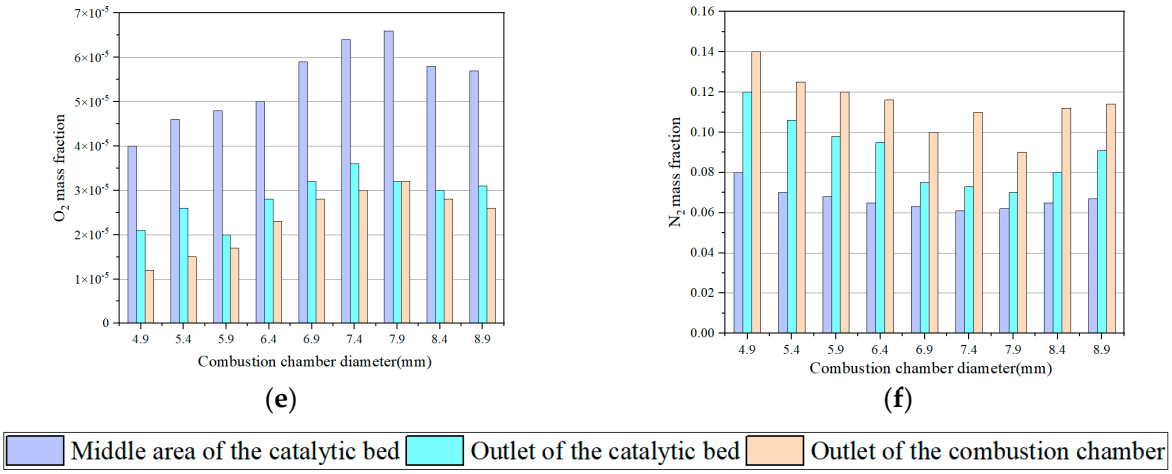

Figure 8. Effect of combustion chamber diameter on temperature, pressure, and concentration of key components: (**a**) temperature; (**b**) pressure; (**c**) AN mass fraction; (**d**) CO_2 mass fraction; (**e**) O_2 mass fraction; (**f**) N_2 mass fraction.

The results showed that when the combustion chamber diameter was 5.4 mm, the reaction high-temperature zone was distributed near the combustion chamber throat, and the highest peak temperature could reach 1550 K. When the combustion chamber diameter continued to decrease to 4.9 mm, the reaction high-temperature zone spread to the combustion chamber area, and the highest peak temperature was 1450 K. When the diameter of the combustion chamber is 6.4 mm, the high-temperature zone of the reaction is concentrated near the entrance of the combustion chamber, and the highest peak temperature can reach 1600 K. When the diameter of the combustion chamber is 6.9 mm, the temperature distribution is similar to that at 6.4 mm, but the peak temperature reaches 1760 K. When the diameter of the combustion chamber is changed from 7.9 mm to 8.9 mm, the temperature of the combustion chamber starts to decrease and the concentration of carbon oxides in the combustion chamber also decreases. The gas combustion pressure in the combustion chamber is significantly affected by the diameter of the combustion chamber. With the increase in combustion chamber diameter, the combustion pressure gradually decreases [3,32]. The results show that the design of the combustion chamber diameter plays an important role in controlling the temperature distribution. The combustion chamber diameter also has an effect on the component distribution of the ADN-based thruster at different sections. The small diameter of the combustion chamber leads to fast flow, and the methanol in the combustion chamber cannot be completely decomposed [21].

The thruster-specific impulse and thrust values for different combustion chamber diameters are given in Figure 9. The results show that the specific impulse and thrust of the thruster reach the maximum value at the combustion chamber diameter of 7.9 mm. As the combustion chamber diameter increases, the rising trend of the calculated specific impulse and thrust values starts to flatten out. The maximum value of specific impulse was 206.6 s at a combustion chamber diameter of 7.9 mm, and the decrease in combustion chamber diameter has a greater effect on the specific impulse of the thruster than the increase in chamber diameter.

3.3. Effects of Combustion Chamber Length on Decomposition and Combustion Characteristics

In order to study the effect of combustion chamber length on the operation of ADN-based thruster, the combustion chamber lengths were set to 5, 7, 9, and 11 mm, respectively. The temperature, velocity, and component distributions of the reactants ADN and intermediate products CO in the thruster axis are given in Figure 10. As the combustion chamber length decreases, the decomposition region of ADN gradually becomes longer, especially when the combustion chamber length is 5 mm, the decomposition region of

ADN becomes significantly longer. The change in the combustion chamber length has little effect on the temperature peak of the gas in the combustion chamber, but the area of the high-temperature region increases as the combustion chamber length increases. When the combustion chamber length is 11 mm, at a distance of 0.01 m from the inlet length, the mass of the CO fraction reaches a maximum value of 0.26, the combustion chamber length increases, the gas injection velocity increases, and the gas injection velocity was lowest when the combustion chamber length was 5 mm, while the gas injection velocity was close for the combustion chamber length of 7 mm to 11 mm.

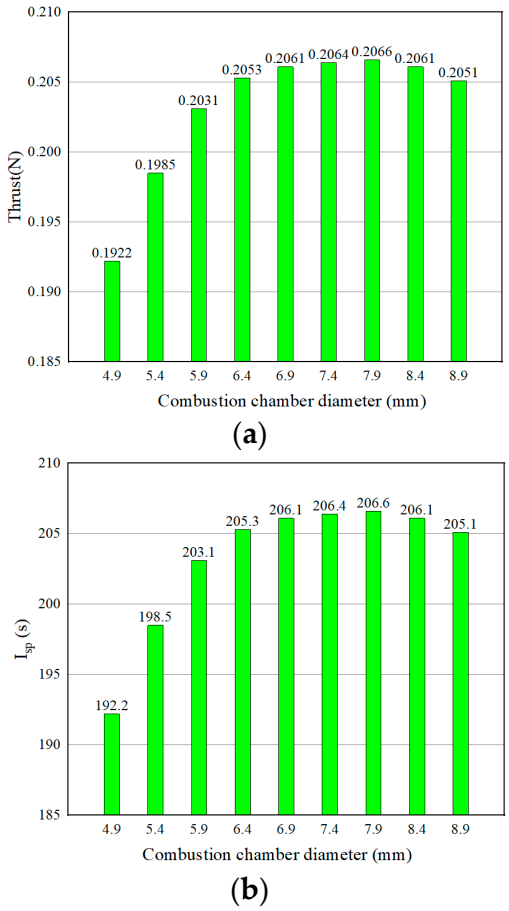

Figure 9. Specific impulse and thrust of thrusters with different combustion chamber diameters: (**a**) specific impulse; (**b**) thrust.

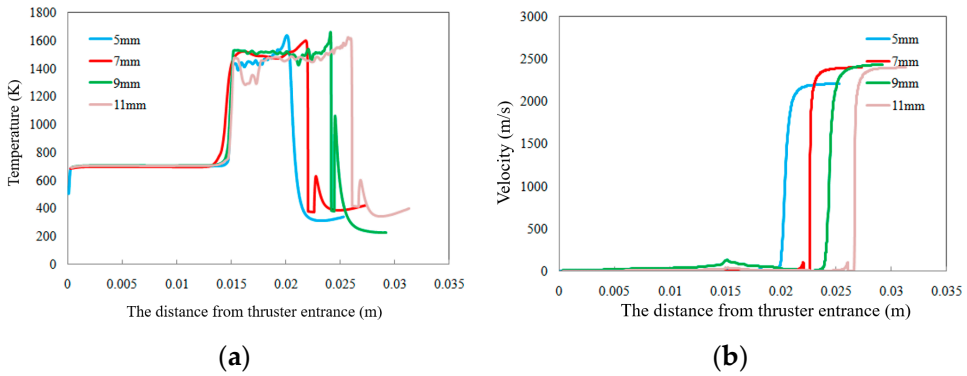

Figure 10. *Cont.*

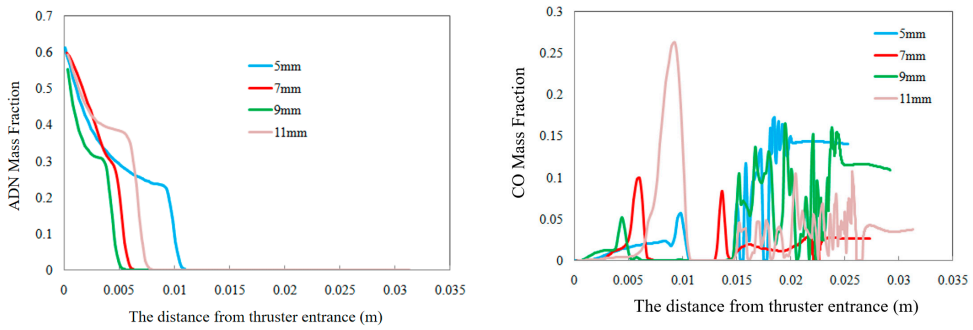

(**c**) (**d**)

Figure 10. Effect of combustion chamber length on the distribution of components, temperature, and gas velocity along the thruster axis: (**a**) temperature; (**b**) velocity; (**c**) ADN mass fraction; (**d**) CO mass fraction.

According to Figure 11, it can be seen that when the combustion chamber length is changed from 7 mm to 15 mm, the thrust and specific impulse both increase gradually and then decrease. When the combustion chamber length is 5 mm, the specific impulse and thrust of the thruster decrease significantly, which seriously affects the combustion performance of the thruster.

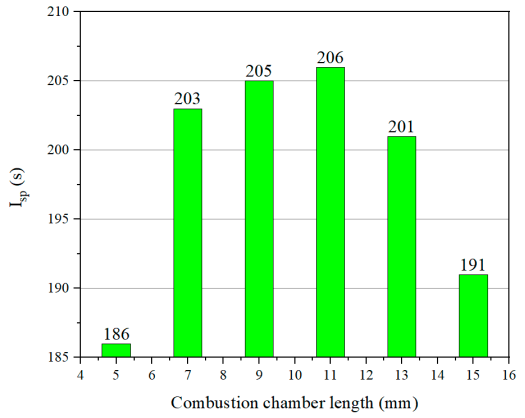

(**a**)

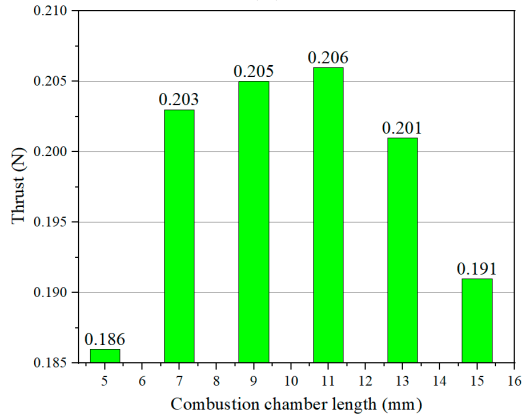

(**b**)

Figure 11. Specific impulse and thrust of different combustion chamber lengths: (**a**) specific impulse; (**b**) thrust.

4. Conclusions

In this paper, the effect of combustion chamber geometrical parameters (length, diameter) on the catalyst decomposition and combustion processes in ADN-based thrusters is investigated using numerical simulations. The main conclusions are as follows:

(1) The results show that the two geometrical parameters of combustion chamber length and diameter have significant effects on the temperature, pressure, and concentration of key product components in the thruster. By comparing the specific impulse and thrust at various geometrical parameters, it is found that the improvement of thruster performance tends to level off with the increase in combustion chamber length and diameter, and there exists a theoretical optimum design value to achieve the best performance of the thruster;

(2) Because of the wall effect, the decomposition rate of an ADN near the wall is slower than that in the center of the catalytic bed, and the decomposition of an ADN is mainly in the catalytic bed area, while the oxidation reaction of methanol is concentrated in the combustion chamber.

Author Contributions: Writing—original draft, Y.H.; Writing—review & editing, Y.Y.; Data curation, X.L.; Investigation, J.C. All authors have read and agreed to the published version of the manuscript.

Funding: The research is supported by the Advanced Space Propulsion Laboratory of BICE and Beijing Engineering Research Center of Efficient and Green Aerospace Propulsion Technology (LabASP-2020-08).

Data Availability Statement: Not applicable.

Acknowledgments: The test data were supported by the Beijing Institute of Control Engineering, China.

Conflicts of Interest: The authors declare no conflict of interest.

Nomenclature

AN	hydroxylamine nitrate	$C_{i,s}$	concentrations of component i on the droplet surface
Yd	mass fraction of the droplets	$C_{i,\infty}$	concentrations of component i inside the droplet
$\overline{d}$	mean diameter	P_t	pressure of evaporation
n	propagation parameter	x_i	volume fraction of component i in the droplet
m_i	the mass of component i in the droplet	d_p	droplet diameter
$k_{c,i}$	mass transport coefficient of component i	k_∞	thermal conductivity of the continuous phase
A_p	surface area of the droplet	$c_{p\infty}$	specific heat capacity of the continuous phase
$M_{w,i}$	molecular weight of component i	f	fluid
s	solid	γ	porosity of porous media
k_f	Fluid-phase thermal conductivity	k_s	Solid-phase thermal conductivity
h_{fs}	thermal conductivity between fluid and solid	A_{fs}	Fluid–solid interfacial density
ρ	solid density	h	sensible enthalpy
k	solid heat transfer coefficient	T	solid temperature
q^m	volume source term	q	heat flow
q_f	heat flow of fluid	q_s	heat flow of solid
I_{sp}	specific impulse	DPM	discrete phase model
UDF	User-defined function		

References

1. Whitmore, A.; Merkley, P.; Eilers, D.; Judson, I. Development and Testing of a Green Monopropellant Ignition System. In Proceedings of the 49th AIAA/ASME/SAE/ASEE Joint Propulsion Conference and Exhibit, San Jose, CA, USA, 15–17 July 2013.
2. Freudenmann, D.; Ciezki, H.K. ADN and HAN-based monopropellants-A minireview on compatibility and chemical stability in aqueous media. *Explos. Pyrotech.* **2019**, *44*, 1084–1089. [CrossRef]
3. Yu, Y.-S.; Li, G.-X.; Zhang, T.; Chen, J.; Wang, M. Effects of catalyst-bed's structure parameters on decomposition and combustion characteristics of an ammonium dinitramide (ADN)-based thruster. *Energy Convers. Manag.* **2015**, *106*, 566–575. [CrossRef]
4. Yang, R.; Thakre, P.; Yang, V. Thermal Decomposition and Combustion of Ammonium Dinitramide (Review). *Combust. Explos. Shock Waves* **2005**, *41*, 657–679. [CrossRef]
5. Oliveira, J. ADN-The new oxidizer around the corner for an environmentally friendly smokeless propellant. *J. Aerosp. Technol. Manag.* **2009**, *1*, 153–160.
6. Handy, S. *Applications of Ionic Liquid in Science and Technology*; InTech Publishing: New York, NY, USA, 2011.
7. Jharapla, P.K.; Vaitheeswaran, G.; Gupta, M.; Mittal, R. Comparative study of electronic structure, optical properties, lattice dynamics and thermal expansion behaviour of energetic ammonium and potassium dinitramide salts. *Mater. Chem. Phys.* **2021**, *267*, 124645. [CrossRef]
8. Yao, Z.; Zhang, W.; Wang, M.; Chen, J.; Shen, Y.; Wei, Y.; Yu, X.; Li, F.; Zeng, H. Tunable diode laser absorption spectroscopy measurements of high-pressure ammonium dinitramide combustion. *Aerosp. Sci. Technol.* **2015**, *45*, 140–149. [CrossRef]
9. Anflo, K.; Crowe, B. In-space demonstration of an ADN-based propulsion system. In Proceedings of the 47th AIAA/ASME/SAE/ASEE Joint Propulsion Conference & Exhibit, San Diego, CA, USA, 31 July–3 August 2011.
10. Izato, Y.-I.; Miyake, A. Detailed kinetic model for ammonium dinitramide decomposition. *Combust. Flame* **2018**, *198*, 222–229. [CrossRef]
11. Wingborg, N.; Eldsäter, C.; Skifs, H. Formulation and characterization of ADN-based liquid monopropellants. In Proceedings of the 41th AIAA/ASME/SAE/ASEE Joint Propulsion Conference & Exhibit, Tucson, AZ, USA, 10–13 July 2004.
12. Jones, D.E.G.; Kwok, Q.S.M.; Vachon, M.; Badeen, C.; Ridley, W. Characterization of ADN and ADN-Based Propellants. *Propellants Explos. Pyrotech.* **2005**, *30*, 140–147. [CrossRef]
13. Wingborg, N. Heat of formation ADN-based liquid monopropellants. *Propellants Explos. Pyrotech.* **2019**, *44*, 1090–1095. [CrossRef]
14. Wingborg, N.; Johansson, M.; Bodin, L. ADN-based liquid monopropellants: Propellant selection and initial thruster development. In Proceedings of the 3rd International Conference on Green Propellants for Space Propulsion, Futuroscope, France, 17–20 September 2006.
15. Jing, L.; You, X.; Huo, J.; Zhu, M.; Yao, Z. Experimental and numerical studies of ammonium dinitramide based liquid propellant combustion in space thruster. *Aerosp. Sci. Technol.* **2017**, *69*, 161–170. [CrossRef]
16. Grönland, T.A.; Anflo, K.; Bergman, G. ADN-based propulsion for spacecraft-Key requirements and experimental verification. In Proceedings of the 40th AIAA/ASME/SAE/ASEE Joint Propulsion Conference & Exhibit, Fort Lauderdale, FL, USA, 11–14 July 2004.
17. Farhat, K.; Kappenstein, C.; Batonneau, Y. Thermal and catalytic decomposition of AN-, ADN and HNF-based ionic monopropellants. In Proceedings of the 44th AIAA/ASME/SAE/ASEE Joint Propulsion Conference & Exhibit, Hartford, CT, USA, 21–23 July 2008.
18. Amrousse, R.; Hori, K.; Fetimi, W. HAN and ADN as liquid ionic monopropellants: Thermal and catalytic decomposition processes. *Appl. Catal. B Environ.* **2012**, *127*, 121–128. [CrossRef]
19. Kim, J.W.; Baek, S.; Jung, Y.; Yoon, W.; Ban, H.S.; Kwon, S. An alternative ADN based monopropellant mixed with tetraglyme. *Acta Astronaut.* **2021**, *178*, 241–249. [CrossRef]
20. Zhang, T.; Li, G.; Yu, Y.; Sun, Z.; Wang, M.; Chen, J. Numerical simulation of ammonium dinitramide (ADN)-basednon-toxic aerospace propellant decomposition and combustion in a monopropellant thruster. *Energy Convers. Manag.* **2014**, *87*, 965–974. [CrossRef]
21. Chen, J.; Li, G.; Zhang, T.; Liu, Y.; Yang, R.; Chen, Y. Catalytic bed slenderness ratio and ADN/methanol ratio for decomposition and combustion characteristics within ammonium dinitramide (ADN)-based green aerospace thruster. *Chin. J. Chem. Eng.* **2019**, *27*, 1159–1165. [CrossRef]
22. Bingue, J.P.; Saveliev, A.V.; Fridman, A.A. Hydrogen production in ultra-rich filtration combustion of methane and hydrogen sulfide. *Int. J. Hydrog. Energ.* **2002**, *27*, 643–649. [CrossRef]
23. Koopmans, R.J.; Shrimpton, J.S.; Roberts, G.T. A one-dimensional multicomponent two-fluid model of a reacting packed bed including mass, momentum and energy interphase transfer. *Int. J. Multiph. Flow* **2013**, *57*, 10–28. [CrossRef]
24. Hitt, D.L.; Zhou, X. One-dimensional modeling of catalyzed H_2O_2 decomposition in microchannel flows. In Proceedings of the 33rd AIAA Fluid Dynamics Conference and Exhibit, Orlando, FL, USA, 23–26 June 2003.
25. Kuwahara, F.; Shirota, M.; Nakayama, A. A numerical study of interfacial convective heat transfer coefficient in two-energy equation model for convection in porous media. *Int. J. Heat Mass Transf.* **2001**, *44*, 1153–1159. [CrossRef]
26. Hou, B.; Wang, X.; Li, T. Steady-state behavior of liquid fuel hydrazine decomposition in packed bed. *AIChE J.* **2015**, *61*, 1064–1080. [CrossRef]
27. Yu, Q.; Yang, Y.; Wang, Z.; Zhu, H. Modeling and parameter sensitivity analysis of fluidized bed solid particle/sCO_2 heat exchanger for concentrated solar power plant. *Appl. Therm. Eng.* **2021**, *197*, 117429. [CrossRef]

28. Sun, Y.N.; Gao, D.R.; Zhang, Z.Y. Study on flow field and temperature field characteristics of gas-liquid two-fluid snowmaking nozzle. *Int. J. Hydromechatron.* **2020**, *1*, 1. [CrossRef]
29. Gunawan, R.; Zhang, D. Thermal stability and kinetics of decomposition of ammonium nitrate in the presence of pyrite. *J. Hazard. Mater.* **2009**, *165*, 751–758. [CrossRef]
30. Korobeinichev, O.P.; Bolshova, T.A.; Paletsky, A.A. Modeling the chemical reactions of ammonium dinitramide (ADN) in a flame. *Combust. Flame* **2001**, *126*, 1516–1523. [CrossRef]
31. Foustoukos, D.I.; Stern, J.C. Oxidation pathways for formic acid under low temperature hydrothermal conditions: Implications for the chemical and isotopic evolution of organics on Mars. *Geochim. Cosmochim. Acta* **2012**, *76*, 14–28. [CrossRef]
32. Heo, S.; Jo, S.; Yun, Y. Effect of dual-catalytic bed using two different catalyst sizes for hydrogen peroxide thruster. *Aerosp. Sci. Technol.* **2018**, *78*, 26–32. [CrossRef]